Electronic Journal of Biotechnology 83 (2026) 100724

Contents lists available at ScienceDirect

Electronic Journal of Biotechnology

journal homepage: www.elsevier.com/locate/ejbt

Research article

Oxidative stress gene signature associated with vitiligo: A multi-algorithm machine learning and Mendelian randomization validationa ☆

Yuan Xia [a,b], Lin Liu [a,b], Hucheng Zhou [a], Lingli Fang [b,c], Yanyan Chen [a,b], Hengheng Fan [a,b], Yuyun Xiong [a,b,*], Yumei Li [a,b,c,*]

[a] Department of Dermatology, Affiliated Hospital of Jiangsu University, Zhenjiang, Jiangsu, China
[b] Institute of Regenerative Medicine, Jiangsu University, Zhenjiang, Jiangsu, China
[c] The First Clinical Medical School, Inner Mongolia Medical University, Hohhot, China

GRAPHICAL ABSTRACT

Oxidative stress gene signature associated with vitiligo: A multi-algorithm machine learning and Mendelian randomization validation.

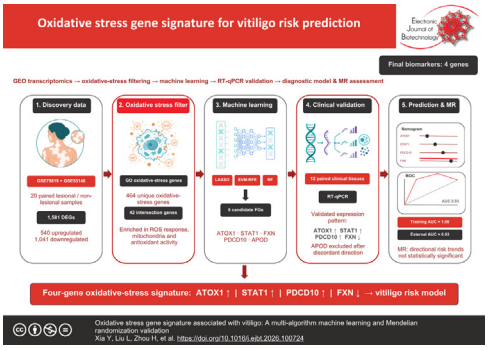

ARTICLE INFO

Article history:
Received 7 December 2025
Accepted 28 April 2026
Available online 28 July 2026

Keywords:
ATOX1
Biomarkers
Differentially expressed genes
FXN
Machine learning
Mendelian randomization
Oxidative stress

ABSTRACT

Background: Vitiligo is a common depigmentation disorder that affects approximately 1–2% of the global population. Oxidative stress plays a crucial role in its pathogenesis, yet systematic identification of oxidative stress-related biomarkers remains limited. This study aimed to identify and validate oxidative stress-related biomarkers for vitiligo and to construct a risk prediction model using bioinformatics, machine learning, and Mendelian randomization approaches.

Results: Through integration of high-throughput sequencing data, 1,581 differentially expressed genes were identified, of which 42 intersected with known oxidative stress-related genes. Three machine learning algorithms converged on five candidate genes. Real-time polymerase chain reaction validation in paired vitiligo lesional and non-lesional skin tissues confirmed the significant upregulation of *ATOX1*, *STAT1*, and *PDCD10* and downregulation of *FXN* ($p < 0.05$). A risk prediction nomogram based on these four genes achieved high accuracy in the training dataset (area under the curve = 1.00) and an independent validation dataset (area under the curve = 0.93). *PDCD10* demonstrated the strongest individual

☆ Audio abstract available in Supplementary material.

Peer review under responsibility of Pontificia Universidad Católica de Valparaíso.

* Corresponding authors.
E-mail addresses: xyybear2004@hotmail.com (Y. Xiong), yumeili@ujs.edu.cn (Y. Li).

https://doi.org/10.1016/j.ejbt.2026.100724

PDCD10
Risk prediction model
STAT1
Vitiligo

discriminatory performance (area under the curve = 0.820) in external validation. Mendelian randomization analysis indicated that *ATOX1*, *STAT1*, and *PDCD10* had odds ratios greater than 1, suggesting a potential trend toward increased vitiligo risk, although the associations did not reach statistical significance.
Conclusions: This study identified *ATOX1*, *STAT1*, *FXN*, and *PDCD10* as oxidative stress-related biomarkers for vitiligo. The four-gene risk prediction model demonstrated promising accuracy, with potential implications for early detection and personalized treatment strategies, pending further validation in larger cohorts.

How to cite: Xia Y, Liu L, Zhou H, et al. Oxidative stress gene signature associated with vitiligo: A multi-algorithm machine learning and Mendelian randomization validation. Electron J Biotechnol 2026;83. https://doi.org/10.1016/j.ejbt.2026.100724.

1. Introduction

Vitiligo, characterized by white patchy skin lesions, predominantly in the nonsegmental form, is a common depigmentation disorder. Statistics indicate that vitiligo affects approximately 1% of the global population, increasing to 1.1–2% in Asians [1]. Nonsegmental vitiligo, the most prevalent subtype, accounts for approximately 85–90% of all cases and is characterized by bilateral, often symmetrical depigmentation patches that tend to enlarge over time [2]. Vitiligo poses a significant challenge, with recurrence rates of facial and neck skin lesions reaching as high as 88.5% [2]. Vitiligo is a hereditary, multifactorial genetic disorder characterized by familial aggregation, with approximately 80% of the risk attributed to genetic factors [3,4,5]. Therefore, the search for methods to predict the risk of vitiligo onset is of paramount importance in clinical practice.

When exposed to harmful stimuli, oxidative stress exceeds the antioxidative capacity, disrupting the balance and leading to the excessive production of reactive oxygen species (ROS) within the body. Previous studies have shown that ROS levels in the blood and skin lesions of patients with vitiligo are significantly elevated [6]. Multiple factors and mechanisms have been implicated in the pathogenesis of vitiligo, including immune responses, oxidative stress, gut microbiota dysbiosis, epigenetics, and chemical or drug induction [5,7]. Among these, the interplay between oxidative stress and the immune response has gained significant attention in recent scholarly discussions. Oxidative stress can serve as an initial pathogenic trigger for melanocyte degeneration and plays a pivotal role in melanocyte damage [7]. Oxidative stress-induced activation of keratinocytes and melanocytes leads to the release of inflammatory mediators, triggering innate and adaptive immune responses and promoting melanocyte death through immune responses. Furthermore, oxidative stress directly damages the mitochondrial respiratory chain and disrupts the normal lipid composition, adversely affecting melanocytes [8].

A retrospective study demonstrated that delaying treatment results in accelerated disease progression and increased recurrence rates [9]. An onset age above 12 years and an extended disease course contribute to treatment failure and a poorer prognosis [10]. These clinical observations underscore the importance of early identification of at-risk individuals. Clinically, vitiligo severity is assessed on the basis of lesion extent, distribution pattern, disease activity (progressive versus stable), and impact on quality of life [1,5]. Therefore, early detection and treatment are imperative for efficacy. Vitiligo-targeting biomarkers allow for early disease screening and diagnosis, enabling the development of personalized treatment plans. Studies have revealed high expression levels of *TYR*, *TYRP1*, *DCT*, *LARP7*, *CKS2*, and *RRM2* in vitiligo samples, suggesting their candidacy as biomarkers [11,12]. Currently, research on biomarkers of oxidative stress in vitiligo is limited. For example, byproducts of DNA oxidative damage, such as serum 8-hydroxy-2-deoxyguanosine or ischemia-modified albumin, have been explored [13,14]. Despite relevant individual studies, a systematic and comprehensive understanding of oxidative stress-related biomarkers in vitiligo is lacking.

Exploring potential targets could provide a foundation for targeted oxidative stress treatment in patients with vitiligo. Currently, immune function inhibition is a significant component of vitiligo treatment [15]. Tacrolimus, for example, reduces the systemic antioxidant stress response and increases antioxidant capacity, thereby promoting skin pigmentation in patients [16,17,18,19]. Oral or local application of antioxidants, such as vitamin E and acetylcysteine, can induce skin pigmentation in patients with vitiligo. Currently, traditional antioxidants have a relatively low adoption rate in clinical practice, with only 11.8% of patients with vitiligo frequently using them and experiencing inconsistent efficacy [20]. However, research on targeted antioxidant drugs is increasing. Hence, further investigations into the critical genes and pathways of targeted antioxidants hold significant promise for vitiligo treatment.

In summary, this study employed bioinformatics, machine learning, and Mendelian randomization analyses to identify potential genetic markers for oxidative stress-associated vitiligo. These potential biomarkers enable the early detection of vitiligo risk in patients, serving as a foundation for prevention and intervention before or in the early stages of the disease. Furthermore, vitiligo treatment is evolving toward greater precision and targeting of the affected areas. Biomarker detection allows the customization of treatment plans for specific patient groups, aligning with the future direction and trends in healthcare.

2. Materials and methods

2.1. Study design

To identify oxidative stress-related genes in vitiligo and assess their functions, we utilized various R packages for analysis. Initially, we downloaded and organized high-throughput sequencing data from vitiligo samples. We subsequently enriched the dataset via gene set enrichment analysis (GSEA). Next, we conducted a preliminary screening of differentially expressed genes (DEGs) from this dataset and performed functional and pathway enrichment analyses on these genes. We then obtained information on oxidative stress-related genes, determined the intersection between these genes and the DEGs, and analyzed their functional and pathway associations. Next, we subjected the intersecting genes to machine learning analysis to identify feature genes (FGs). To validate the expression of FGs, we collected patient tissue samples and conducted real-time PCR experiments on both vitiligo lesion and non-lesion tissues, resulting in the identification of reliable FGs. Finally, we utilized these FGs to construct and develop a nomogram for a

diagnostic and risk prediction model. We subsequently employed another high-throughput sequencing dataset from vitiligo patients for validation and assessed the accuracy of the FGs and prediction models via receiver operating characteristic (ROC) curves. Furthermore, we conducted Mendelian randomization analysis to investigate the causal relationships and effect values of these FGs in the context of the disease.

2.2. Data collection, processing and enrichment analysis by GSEA

We retrieved high-throughput sequencing data related to vitiligo from the Gene Expression Omnibus (GEO) database (https://www.ncbi.nlm.nih.gov/geo/) [21] and PubMed (https://pubmed.ncbi.nlm.nih.gov/). Two datasets were selected for the discovery cohort: GSE75819 (15 paired lesional and non-lesional skin samples; platform GPL6884, Illumina HumanWG-6 v3.0 expression beadchip) and GSE53146 (5 paired lesional and non-lesional skin samples; platform GPL14951). Both datasets included patients with non-segmental vitiligo. An independent validation dataset, GSE65127 (10 lesional centers and 10 non-lesional tissues; platform GPL570, Affymetrix Human Genome U133 Plus 2.0 Array), was reserved for external model validation. Although the sample sizes of the discovery datasets were modest, they represented the largest publicly available paired lesional–non-lesional vitiligo transcriptomic datasets at the time of analysis. To mitigate the risk of false discoveries associated with small sample sizes, we applied stringent statistical thresholds and validated our findings using an independent dataset and experimental confirmation by real-time PCR.

Upon acquiring raw high-throughput sequencing data from vitiligo samples, we standardized and homogenized the sample classification information and gene expression levels. Given that GSE75819 and GSE53146 were derived from different microarray platforms, inter-platform batch effects were corrected using the ComBat function from the sva R package [22] after initial normalization within each dataset using the limma package [23]. We employed log2 transformation for uniform processing when the original gene expression data showed significant dispersion. Finally, we stored the processed sample classification and gene expression levels separately to ensure their availability for future analyses.

We performed enrichment analysis on the two sets of sample data obtained from the previous step using GSEA 4.3.2 software [24]. We then applied parameter filtering conditions (| normalized enrichment score| $\geq$ 1; nominal p value < 0.05; FDR q value < 0.25) to identify functions or pathways with statistically significant differences.

2.3. Identification of DEGs and enrichment analysis

The limma package was used to identify DEGs between the two groups of sample data, applying thresholds of |log2 fold change| > 0.5 and adjusted p value < 0.05. Additionally, we utilized R packages, such as pheatmap and RColorBrewer for heatmaps and dplyr and ggplot2 for volcano plots.

Gene Ontology (GO) analysis is a common method for studying gene functional enrichment, encompassing biological processes, molecular functions, and cellular components [25]. The Kyoto Encyclopedia of Genes and Genomes (KEGG) contains extensive data on genomes, biological pathways, diseases, chemicals, and drugs [26]. We utilized the clusterProfiler package [27] to conduct GO and KEGG enrichment analyses on the DEGs, considering q values < 0.05 as indicating significant differences. We visualized the results using bubble and bar charts via the GOplot package.

2.4. Screening intersection genes and enrichment analysis

The keyword "oxidative stress" was retrieved from the AmiGO 2 platform (https://amigo.geneontology.org/amigo) [28]. Specifically, we searched for the Gene Ontology term "response to oxidative stress" (GO:0006979) and its child terms, filtering the results by *Homo sapiens*. The gene list was downloaded on June 15, 2023, yielding 465 oxidative stress-related genes before duplicate removal. The intersection of DEGs and oxidative stress genes was obtained using the VennDiagram R package, and a Venn diagram was drawn. As mentioned above, GO and KEGG analyses were performed on the intersecting genes.

2.5. Screening FGs through machine learning algorithms

Machine learning can effectively classify the distinct features of target genes relevant to oxidative stress. In this study, we employed a multi-algorithm consensus approach using three complementary machine learning methods to enhance the robustness and reliability of feature selection. The rationale for combining multiple algorithms is that each method captures different aspects of the data: least absolute shrinkage and selection operator (LASSO) logistic regression performs regularization-based variable selection, support vector machine recursive feature elimination (SVM-RFE) identifies features based on classification margin optimization, and random forest (RF) ranks features according to their contribution to classification tree accuracy. By intersecting the results from all three methods, we retained only those genes consistently identified as important across fundamentally different analytical frameworks, thereby reducing the likelihood of method-specific artifacts and increasing confidence in the selected features [29].

LASSO logistic regression was applied for feature selection and data unification via the glmnet package, with 10-fold cross-validation to determine the optimal regularization parameter (λ) that minimized the mean squared error. SVM-RFE was employed to reduce feature dimensions, and analysis was conducted via the e1071 package with 10-fold cross-validation; the optimal number of features was determined based on classification accuracy and error rate. RF, an ensemble learning method based on classification tree construction, was analyzed using the randomForest package with 500 trees (ntree = 500), and gene importance was ranked by the mean decrease in Gini impurity. The classification performance of each algorithm was assessed using accuracy, sensitivity, specificity, and area under the ROC curve. Genes with higher scores were separately screened using each of the three machine learning methods, and the final FGs were obtained by taking the intersection of the selected genes from all three methods.

2.6. Clinical tissue collection and real-time PCR

Paired vitiligo epidermis and normal skin tissues were obtained through surgical procedures at the Affiliated Hospital of Jiangsu University, China. The study included 12 patients with stable non-segmental vitiligo (5 males and 7 females; age range, 22–56 years; mean age, 36.3 ± 10.8 years). Stable vitiligo was defined as the absence of new lesion development, absence of expansion of existing lesions, and absence of the Koebner phenomenon for a minimum of 6 months prior to enrollment, as assessed by experienced dermatologists [30]. The exclusion criteria included patients in the progressive stage of vitiligo, those with segmental vitiligo, those who had received systemic immunosuppressive or phototherapy treatment within the preceding 3 months, and those who could not tolerate surgical skin incisions. The clinical and demographic characteristics of the study participants are summarized in Table S1. The study was approved by the Human Scientific

Ethics Committee of the Affiliated Hospital of Jiangsu University (approval number: KY2023K1106), and the Declaration of Helsinki guidelines were followed throughout the study. Written informed consent was obtained from all the participants.

Total RNA was isolated using TRIzol and reverse transcribed into cDNA using a RevertAid First Strand cDNA Synthesis Kit according to the manufacturer's instructions. Amplification was performed using a real-time PCR system (Applied Biosystems QuantStudio 3, USA). The entire procedure was performed according to the SYBR Premix Ex Taq kit manual. The $2^{-\Delta\Delta Cq}$ method was used to quantify the expression levels of target genes, with *GAPDH* as the internal control gene. The primers used are listed in Table S2.

2.7. Construction of the diagnostic nomogram and verification via ROC curves

Nomograms can be used to diagnose clinical diseases. The rms package was used to construct a vitiligo diagnosis model based on the expression of FGs using logistic regression. The pROC package was subsequently used to analyze the area under the curve (AUC) of the FGs and diagnostic models to evaluate the accuracy of gene and model predictions. The AUC values were interpreted as follows: $0.5 \leq AUC < 0.7$, low accuracy; $0.7 \leq AUC < 0.9$, moderate accuracy; and $AUC \geq 0.9$, high accuracy.

2.8. Validation from another public dataset

Another high-throughput dataset of patients with vitiligo (GSE65127) was selected and processed to construct the risk prediction model again based on the screened FGs, with the objective of further validation. Finally, ROC curves were used to assess the accuracy of the screened FGs and risk prediction models in this dataset.

2.9. Mendelian randomization analysis

Two-sample Mendelian randomization (MR) was used to evaluate the potential causal relationship between FG expression levels and vitiligo risk. Exposure data (expression quantitative trait loci, eQTLs) for each FG were obtained from the IEU OpenGWAS project database (https://gwas.mrcieu.ac.uk/) [31]. The outcome data for patients with vitiligo were retrieved from the same database. Instrumental variables (single-nucleotide polymorphisms, SNPs) were selected using a genome-wide significance threshold of $p < 5 \times 10^{-8}$. Linkage disequilibrium (LD) pruning was performed using an r^2 threshold of 0.001 and a clumping window of 10,000 kb to ensure the independence of instruments. The F-statistic for each instrument was calculated to assess instrument strength, with $F > 10$ considered adequate to avoid weak-instrument bias. The number of SNPs and mean F-statistics for each gene are shown in Table 1. The primary analysis was performed using the inverse variance weighted (IVW) method via the TwoSampleMR R package [32]. Sensitivity analyses included the MR-Egger method to detect and correct for directional pleiotropy (with the intercept test assessing pleiotropy), the weighted median method providing consistent estimates when up to 50% of instruments were invalid, and Cochran's Q statistic for heterogeneity assessment. The results of the sensitivity analyses are presented in Table S3.

2.10. Statistical methods

All statistical analyses, including LASSO, SVM-RFE, RF, and ROC curve analyses, were performed using R software version 4.2.2 and GraphPad Prism version 9. The significance level was set at $p < 0.05$ for all analyses.

3. Results

3.1. Data collection and processing and GSEA

Original high-throughput data from the vitiligo datasets GSE75819, GSE53146, and GSE65127 were retrieved from the GEO database (Table 2). The 15 pairs of tissues from GSE75819 and the 5 pairs of tissues from GSE53146 were integrated, including 20 diseased and 20 normal tissues. Inter-platform batch effects were corrected using the ComBat method prior to downstream analyses. We obtained 20,819 genes and their expression data, which were used to screen for FGs. We downloaded data from GSE65127 and retrieved 10 vitiligo lesion centers and 10 non-lesion tissues from the dataset. After summarizing the results, 54,675 genes and their expression data were obtained from the database. This dataset was used for the subsequent verification of the FGs. The limma package was used to standardize and unify all data. Owing to the large degree of data dispersion, the data were converted to log2. Finally, the data were saved for subsequent analysis.

We employed GSEA 4.3.2 software to conduct GO and KEGG enrichment analyses on the lesion and normal groups. We filtered the results based on specific criteria, including a nominal p value < 5%, an FDR q-value < 25%, and $|NES| > 1$. Following this analysis, we observed significant associations among genes in the vitiligo lesion group, including those involved in protein neddylation, NOD-like receptor signaling pathway, Toll-like receptor signaling pathway, and RIG-I-like receptor signaling pathway (Fig. 1A–D).

3.2. Identification of DEGs and enrichment analysis

We utilized the limma package to identify 1,581 DEGs, consisting of 540 upregulated genes and 1,041 downregulated ones. These genes are represented by a volcano plot and heatmap for better visualization (Fig. 2A and B). We concurrently conducted GO and KEGG enrichment analyses of the DEGs.

Table 1
Mendelian randomization of feature genes using the inverse variance weighted method.

Gene	GWAS ID	No. of SNPs	Mean F-statistic	OR (95% CI)	*p* value
ATOX1	eqtl-a-ENSG00000177556	5	32.4	1.31 (0.88–1.96)	0.186
STAT1	eqtl-a-ENSG00000115415	4	28.7	1.96 (0.95–4.02)	0.067
FXN	eqtl-a-ENSG00000165060	3	21.5	0.70 (0.05–9.23)	0.789
PDCD10	eqtl-a-ENSG00000114209	3	25.1	2.80 (0.64–12.31)	0.172

OR, odds ratio; CI, confidence interval; SNP, single-nucleotide polymorphism. All 95% CIs cross the null value of 1, indicating that none of the associations reached statistical significance. The OR point estimates suggest directional trends (*ATOX1*, *STAT1*, and *PDCD10* OR > 1; *FXN* OR < 1) that warrant further investigation with larger datasets. All F-statistics exceeded the threshold of 10, indicating adequate instrument strength. Gene names are italicized per standard nomenclature.

Table 2
Detailed information of GEO datasets applied in the study.

Series record	Citation title	Submission year	Last update year	Sample	Platform
GSE75819	Mapping architectural and transcriptional alterations in non-lesional and lesional epidermis in vitiligo	2015	2019	15 lesional skin and 15 normal skin	GPL6884 (Illumina HumanWG-6 v3.0)
GSE53146	CXCL10 is critical for the progression and maintenance of depigmentation in a mouse model of vitiligo	2014	2017	5 lesional skin and 5 normal skin	GPL14951
GSE65127	Transcriptional analysis of vitiligo skin reveals the alteration of WNT pathway: a promising target for repigmenting vitiligo patients	2015	2019	10 lesional skin and 10 normal skin	GPL570 (Affymetrix HGU133 Plus 2.0)

Note: GSE75819 and GSE53146 were used as the discovery cohort (combined n = 20 lesional, 20 nonlesional). GSE65127 was used as the independent validation cohort (n = 10 lesional centers, 10 nonlesional). Inter-platform batch effects between GSE75819 and GSE53146 were corrected using ComBat prior to analysis.

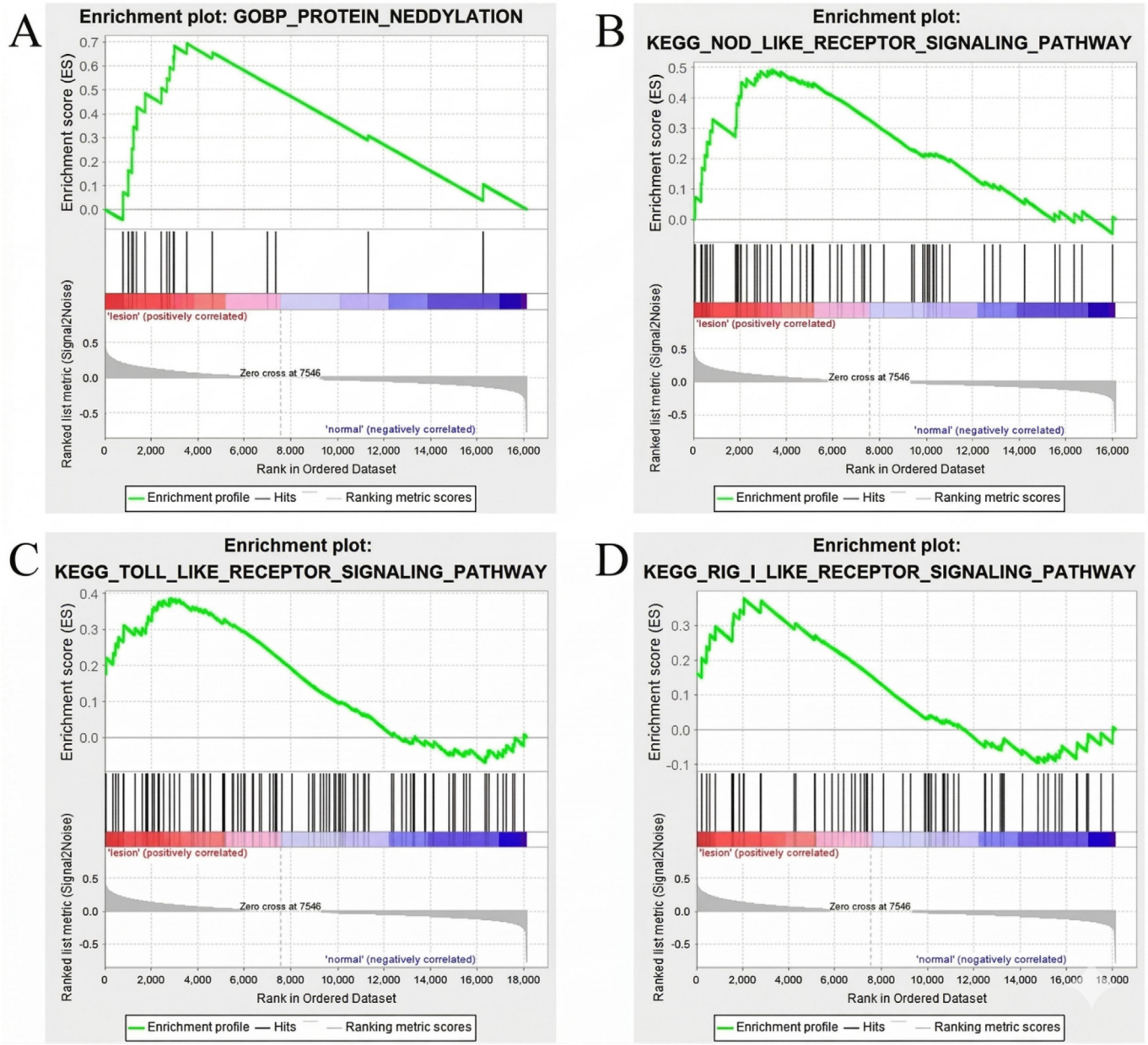

Fig. 1. Gene set enrichment analysis (GSEA) revealed key pathways associated with vitiligo pathogenesis. (A) Protein neddylation (P = 0.008, FDR q = 0.125, |NES| = 1.780). (B) NOD-like receptor signaling pathway (P = 0.011, FDR q = 0.091, |NES| = 1.596). (C) Toll-like receptor signaling pathway (P = 0.019, FDR q = 0.143, |NES| = 1.468). (D) RIG-I-like receptor signaling pathway (P = 0.041, FDR q = 0.173, |NES| = 1.425). NES: normalized enrichment score.

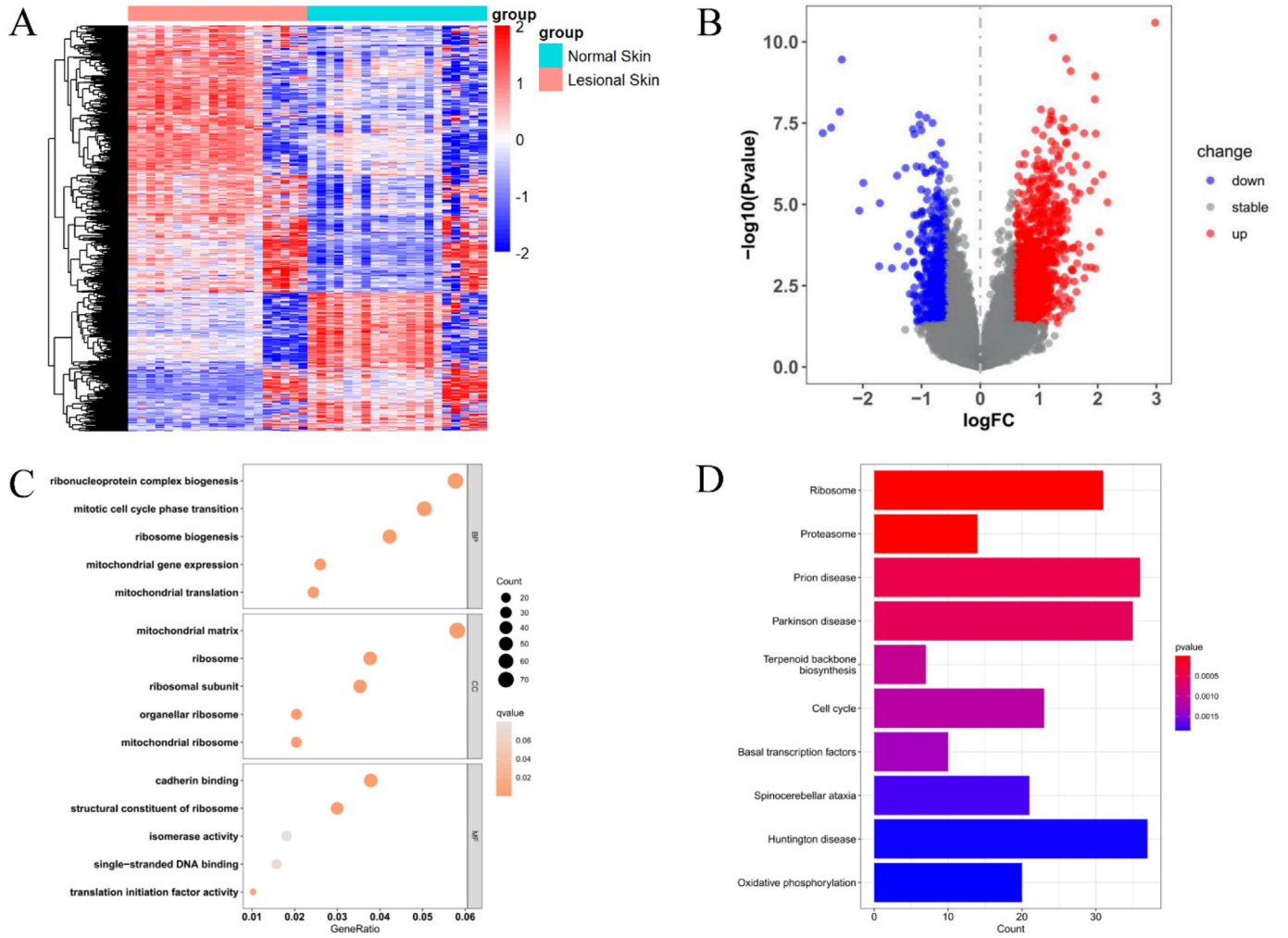

Fig. 2. Identification and functional analysis of differentially expressed genes (DEGs) in vitiligo patients. (A) Heatmap of DEGs. Red indicates upregulation, and blue indicates downregulation. (B) Volcano plot of DEGs. Red dots: upregulated genes; blue dots: downregulated genes; gray dots: genes with stable expression. (C) Gene Ontology (GO) enrichment analysis of DEGs visualized as a bubble plot. Bubble size is correlated with gene count; color intensity indicates statistical significance. (D) Kyoto Encyclopedia of Genes and Genomes (KEGG) pathway enrichment analysis of DEGs presented as a bar chart, arranged by *p* value significance. (For interpretation of the references to colour in this figure legend, the reader is referred to the web version of this article.)

GO enrichment analysis revealed significant associations with the mitochondrial matrix, ribosomes, and other cellular components, as shown in the bubble chart. The KEGG enrichment results, presented as bar graphs, highlighted notable pathways, including oxidative phosphorylation (Fig. 2C and D).

3.3. Intersection between DEGs and oxidative stress genes and enrichment analysis

We obtained 465 oxidative stress-related genes by downloading the data from the AmiGO 2 platform. After removing duplicates, 464 unique genes were identified. We subsequently conducted an intersection analysis between these 464 genes and the 1,581 DEGs, identifying 42 intersection genes (Table 3). A Venn diagram was created to visualize this overlap (Fig. 3A).

We also performed an enrichment analysis of the intersecting genes. The results of the GO enrichment analysis included response to oxidative stress, response to ROS, mitochondrial matrix, and anti-oxidant activity. The enriched KEGG pathways included those related to neurodegeneration-multiple diseases, chemical carcinogenesis-ROS, the adipocytokine signaling pathway, and the prolactin signaling pathway. The findings were plotted as bubble plots and bar graphs (Fig. 3B and C).

3.4. Screening of FGs through machine learning algorithms

We identified the optimal λ value by minimizing the mean squared error in the coefficient map of the LASSO algorithm. Using the selected λ value with the smallest mean squared error, we incorporated it into the regression model, which identified 17 genes (Fig. 4A). The SVM-RFE algorithm ranks the scores of each feature and selects the most suitable number of features for the model. Through 10-fold cross-validation, we found that the 15 selected genes had high accuracy and low error rates (Fig. 4B). The RF algorithm, based on constructing classification trees with 500 trees, yielded 15 important genes quantified by the mean decrease in Gini impurity with a low classification error (Fig. 4C). Using these three machine learning methods, we subsequently narrowed our selection to five FGs: *ATOX1*, *STAT1*, *FXN*, *PDCD10*, and *APOD* (Fig. 4D). Among these genes, the expression of *FXN* and *APOD* decreased, whereas that of *ATOX1*, *STAT1*, and *PDCD10* increased.

3.5. In vitro experimental verification of FGs

RNA was extracted from both vitiligo lesions and normal skin tissues of 12 patients, followed by reverse transcription into cDNA.

Table 3
Expression levels of intersection genes.

Gene	logFC	AveExpr	T	*p* value	adjust. *p* value	B
STAT1	1.028	10.522	4.627	0.000	0.003	2.120
PAWR	1.040	9.084	4.359	0.000	0.005	1.338
ATOX1	0.793	12.126	4.307	0.000	0.006	1.190
HDAC2	1.074	10.448	3.921	0.000	0.012	0.100
ZNF580	−0.702	7.589	−3.903	0.000	0.012	0.049
OXR1	1.177	11.697	3.816	0.000	0.015	−0.190
PDK2	−0.705	7.846	−3.785	0.001	0.016	−0.275
PRDX3	0.908	9.566	3.607	0.001	0.022	−0.755
PNPLA8	0.675	7.920	3.606	0.001	0.022	−0.758
APOD	−1.503	9.476	−3.578	0.001	0.023	−0.832
NDUFA12	1.056	12.058	3.558	0.001	0.024	−0.886
PDCD10	1.010	8.874	3.542	0.001	0.025	−0.928
NUPR1	0.695	11.185	3.276	0.002	0.042	−1.618
ARG1	1.136	11.097	3.113	0.003	0.056	−2.026
EZH2	0.683	8.083	3.045	0.004	0.063	−2.191
PCGF2	−0.642	9.154	−3.036	0.004	0.064	−2.214
ZNF277	1.189	9.545	3.008	0.005	0.066	−2.281
JAK2	0.667	8.372	3.007	0.005	0.066	−2.284
RELA	−0.831	8.240	−2.998	0.005	0.068	−2.306
FXN	−0.616	7.057	−2.793	0.008	0.097	−2.790
CD36	1.189	8.040	2.788	0.008	0.098	−2.800
AIF1	0.687	8.416	2.615	0.013	0.129	−3.190
BAK1	−0.590	8.226	−2.611	0.013	0.129	−3.200
PRDX4	0.628	11.182	2.608	0.013	0.130	−3.205
ANXA1	1.217	12.156	2.577	0.014	0.135	−3.274
PTGS2	1.112	8.740	2.495	0.017	0.152	−3.451
PRODH	−0.689	10.561	−2.492	0.017	0.153	−3.458
ATP13A2	−0.627	8.934	−2.485	0.017	0.155	−3.472
MELK	0.694	7.803	2.481	0.017	0.156	−3.481
ECT2	0.901	8.846	2.409	0.021	0.174	−3.630
NFE2L2	0.792	11.548	2.401	0.021	0.176	−3.647
NUDT2	0.860	9.631	2.340	0.024	0.190	−3.773
MGST1	0.721	7.620	2.325	0.025	0.194	−3.804
MSRA	−0.597	9.403	−2.296	0.027	0.202	−3.861
RWDD1	1.353	10.362	2.290	0.027	0.203	−3.873
PON2	0.832	10.559	2.289	0.027	0.204	−3.877
NCOA7	0.932	9.545	2.270	0.029	0.209	−3.913
NET1	0.753	10.104	2.270	0.029	0.209	−3.914
PRNP	0.749	12.624	2.249	0.030	0.215	−3.955
SESN3	0.668	7.594	2.232	0.031	0.220	−3.989
SOD1	0.634	12.496	2.157	0.037	0.243	−4.133
PARK7	0.854	11.305	2.108	0.041	0.259	−4.227

FC, fold change; AveExpr, average expression. Gene names are italicized per standard nomenclature.

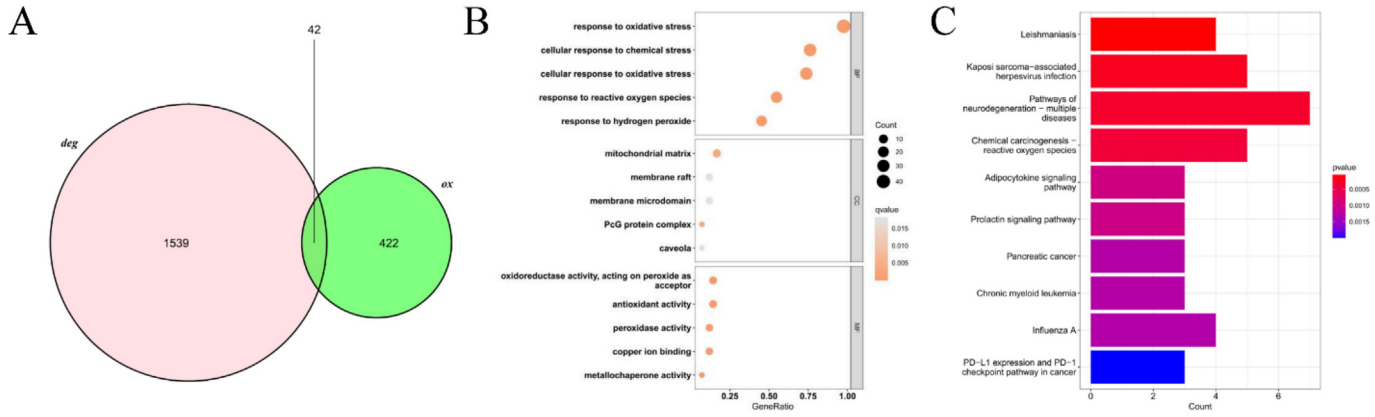

Fig. 3. Intersection analysis of DEGs and oxidative stress-related genes revealed potential vitiligo biomarkers. (A) Venn diagram showing the overlap between DEGs and oxidative stress-related genes. (B) GO enrichment analysis of the intersection genes visualized as a bubble plot. Bubble size is correlated with gene count; color intensity indicates statistical significance. (C) KEGG pathway enrichment analysis of intersection genes presented as a bar chart, arranged by *p* value significance.

Subsequently, real-time PCR experiments were conducted to compare the FG expression levels in the two tissue types. The results revealed a significant increase in the expression of *ATOX1*, *STAT1*, *PDCD10*, and *APOD* in vitiligo lesions ($p < 0.05$), whereas the expression of *FXN* was significantly decreased in vitiligo lesions ($p < 0.05$) (Fig. 5). Except for *APOD*, the expression of the other

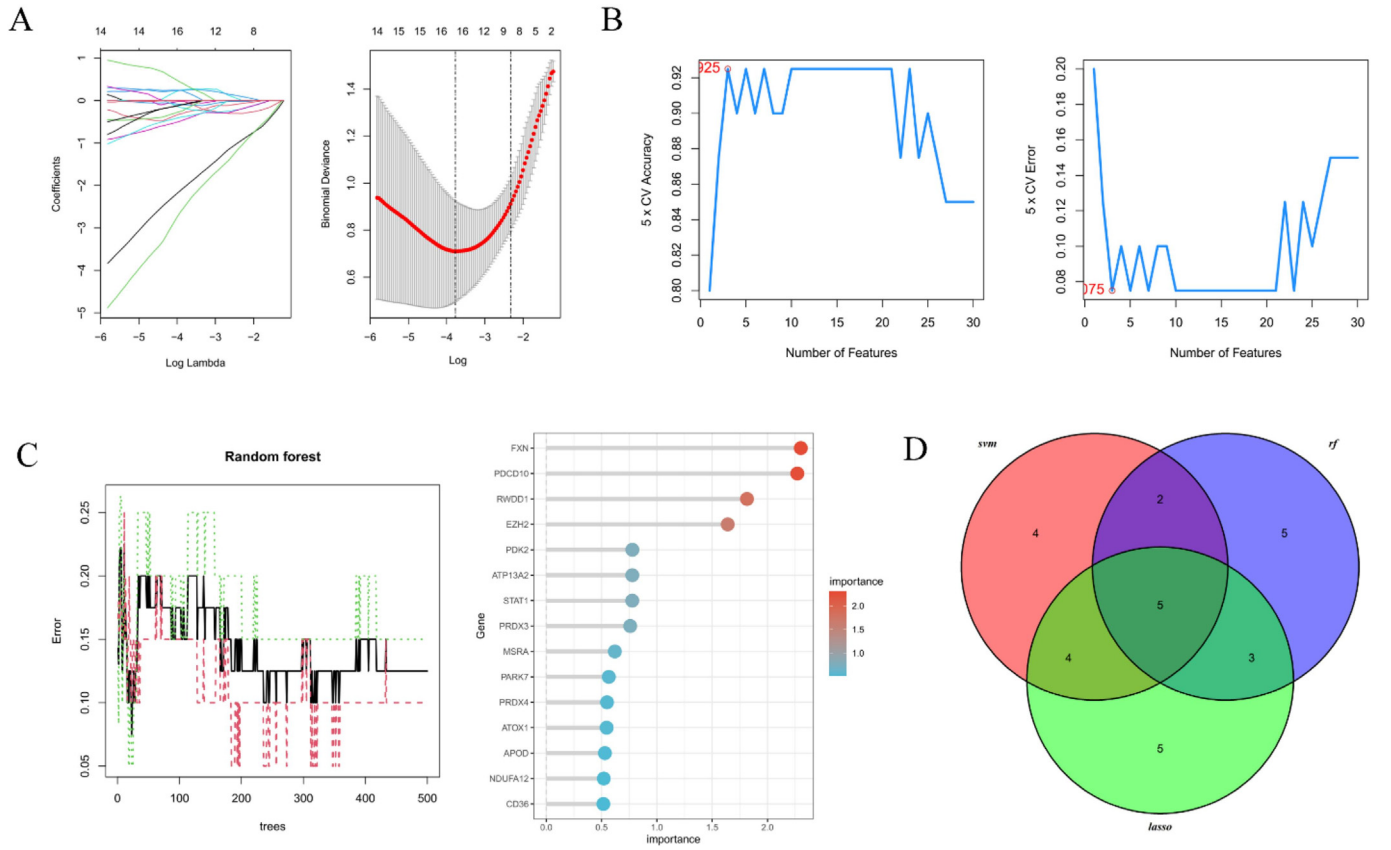

Fig. 4. Machine learning approach for feature gene (FG) selection in vitiligo. (A) Least absolute shrinkage and selection operator (LASSO) logistic regression analysis. (B) Support vector machine recursive feature elimination (SVM-RFE) algorithm results. (C) Random forest (RF) algorithm results. (D) Venn diagram showing the overlap of genes identified by the three machine learning approaches, yielding the final set of FGs.

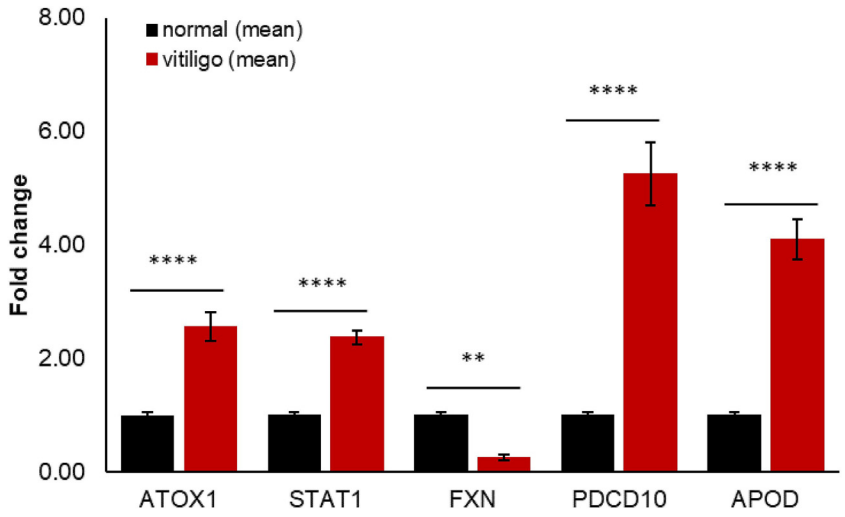

Fig. 5. Experimental validation of selected feature gene expression in vitiligo lesions and normal skin tissues. mRNA expression levels of *ATOX1*, *STAT1*, *FXN*, *PDCD10*, and *APOD* in vitiligo lesions and normal skin tissues, as measured by real-time PCR. The expression levels were normalized to those of *GAPDH*. $^{**}p < 0.01$, $^{****}p < 0.0001$.

FGs matched the predicted results, confirming that *ATOX1*, *STAT1*, *FXN*, and *PDCD10* are FGs associated with oxidative stress in vitiligo.

3.6. Construction and validation via ROC curves

Based on the four identified FGs, we developed a vitiligo risk prediction model and constructed a nomogram. These genes were assigned different scores based on their expression levels. The total score, obtained by summing each gene score, corresponded to different risk levels (Fig. 6A). A higher total score indicates a greater risk of developing vitiligo. To assess the accuracy and sensitivity of the diagnostic model, we used ROC curves, and the AUC was found to be 1.00, indicating perfect accuracy in the training dataset (Fig. 6B). Similarly, we continued to evaluate the four FGs using ROC analysis and found that *ATOX1* (AUC = 0.873), *STAT1*

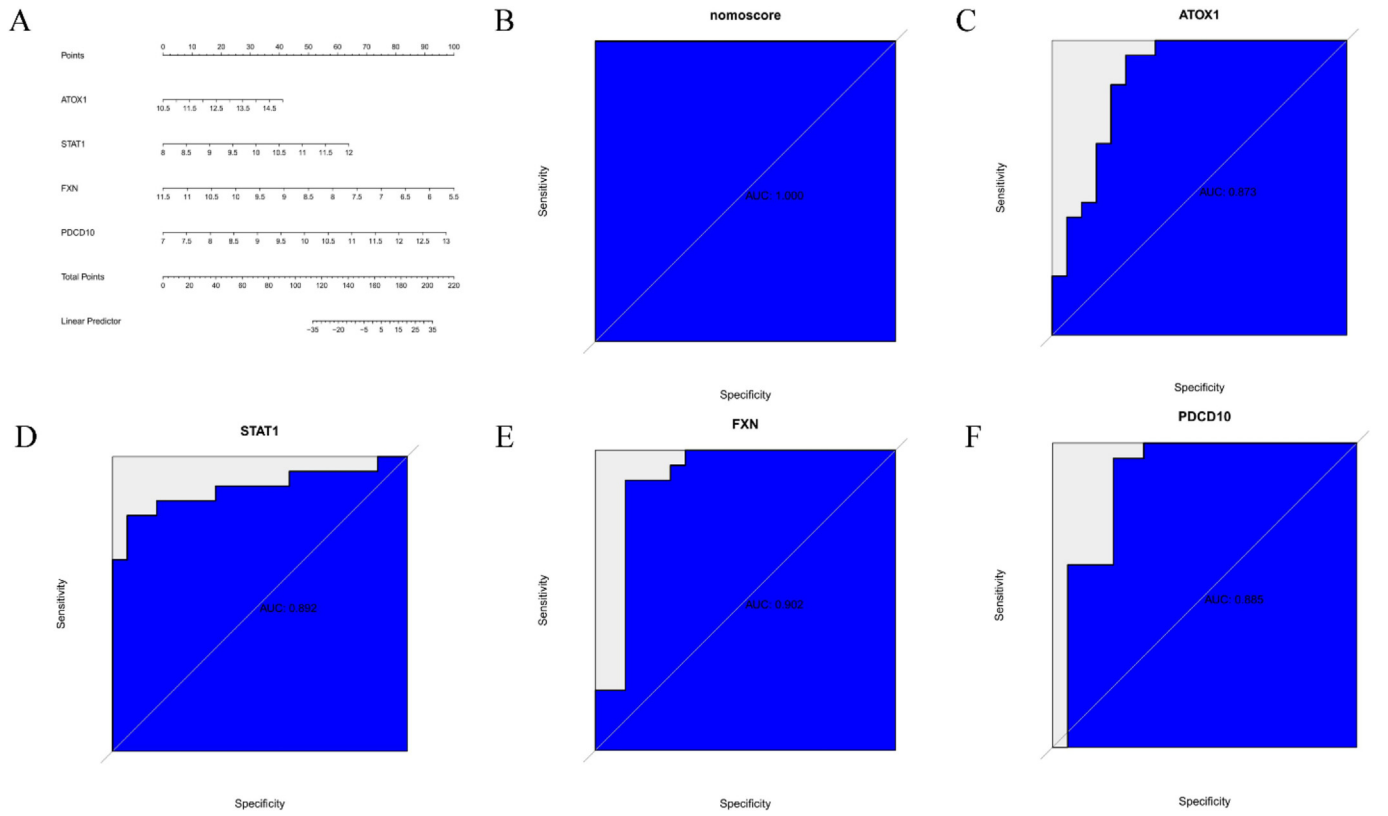

Fig. 6. Development and validation of a diagnostic nomogram for vitiligo risk prediction using the initial dataset. (A) Diagnostic nomogram based on FG expression. (B) Receiver operating characteristic (ROC) curve validation of the diagnostic nomogram. (C–F) Individual ROC curves for *ATOX1*, *STAT1*, *FXN*, and *PDCD10*. AUC interpretation: 0.5 ≤ AUC < 0.7: low accuracy; 0.7 ≤ AUC < 0.9: moderate accuracy; AUC ≥ 0.9: high accuracy.

(AUC = 0.892), *FXN* (AUC = 0.902), and *PDCD10* (AUC = 0.885) demonstrated high accuracy and sensitivity (Fig. 6C–F).

3.7. Another public dataset validation and ROC curve testing

We retrieved the high-throughput dataset GSE65127 from the GEO database and standardized the data. We subsequently employed 10 pairs of samples within the lesion center and non-lesion area to validate the gene information, yielding a dataset encompassing 54,675 genes and their respective expression levels. Using the four FGs, we developed a new risk prediction model, and upon validation via ROC curve analysis, the AUC remained at 0.93, indicating high accuracy (Fig. 7A and B). The accuracy of individual FGs was also evaluated, with *ATOX1* (AUC = 0.480), *STAT1* (AUC = 0.570), *FXN* (AUC = 0.530), and *PDCD10* (AUC = 0.820) obtained. Notably, *PDCD10* demonstrated the highest individual accuracy, indicating that *PDCD10* could be considered the most robust single-gene biomarker among the four FGs (Fig. 7C–F). However, it should be noted that *ATOX1*, *STAT1*, and *FXN* individually showed weak discriminatory performance (AUC < 0.7) in this external dataset, suggesting that the predictive strength of the model relies on the combined contribution of all four genes rather than on any single gene alone (see Section 4, Discussion).

3.8. Mendelian randomization analysis of four FGs

Datasets corresponding to the four FGs were retrieved from the IEU OpenGWAS project database. Utilizing the inverse variance weighted method, we conducted an analysis resulting in the calculation of the respective odds ratios (ORs) and 95% confidence intervals (CIs), which are summarized in Table 1. The point estimates indicated that the OR values for *ATOX1* (OR = 1.31, 95% CI: 0.88–1.96, P = 0.186), *STAT1* (OR = 1.96, 95% CI: 0.95–4.02, P = 0.067), and *PDCD10* (OR = 2.80, 95% CI: 0.64–12.31, P = 0.172) were greater than 1, while *FXN* (OR = 0.70, 95% CI: 0.05–9.23, P = 0.789) had a point estimate below 1. However, all 95% CIs included the null value of 1, indicating that none of these associations were statistically significant. Therefore, these MR results should be interpreted as suggestive of potential directional trends rather than definitive evidence of causal relationships. The wide CIs, particularly for *FXN* and *PDCD10*, likely reflect limited statistical power due to the number and strength of the available instrumental variables. Sensitivity analyses, including MR-Egger regression and the weighted median method, yielded directionally consistent estimates, and no evidence of significant pleiotropy was detected (MR-Egger intercept $p > 0.05$ for all genes; Table S3).

4. Discussion

In this study, our primary objective was to investigate the relationship between gene expression patterns and oxidative stress in patients with vitiligo. We initiated our research by screening gene expression data obtained from the high-throughput sequencing of the GSE75819 and GSE53146 datasets in the GEO database. GSEA revealed significant associations between genes in the vitiligo lesion group and pathways related to protein neddylation, NOD-like receptor signaling, Toll-like receptor signaling, and RIG-I-like receptor signaling pathways. We subsequently identified 1,581 DEGs in vitiligo, comprising 540 upregulated and 1,041 downregulated genes. DEGs were primarily enriched in functions related to the mitochondrial matrix, ribosomes, and oxidative phosphorylation, suggesting a pivotal role of oxidative stress in the pathogenesis of vitiligo. To further explore the critical genes, we intersected the 1,581 differentially expressed genes with 464

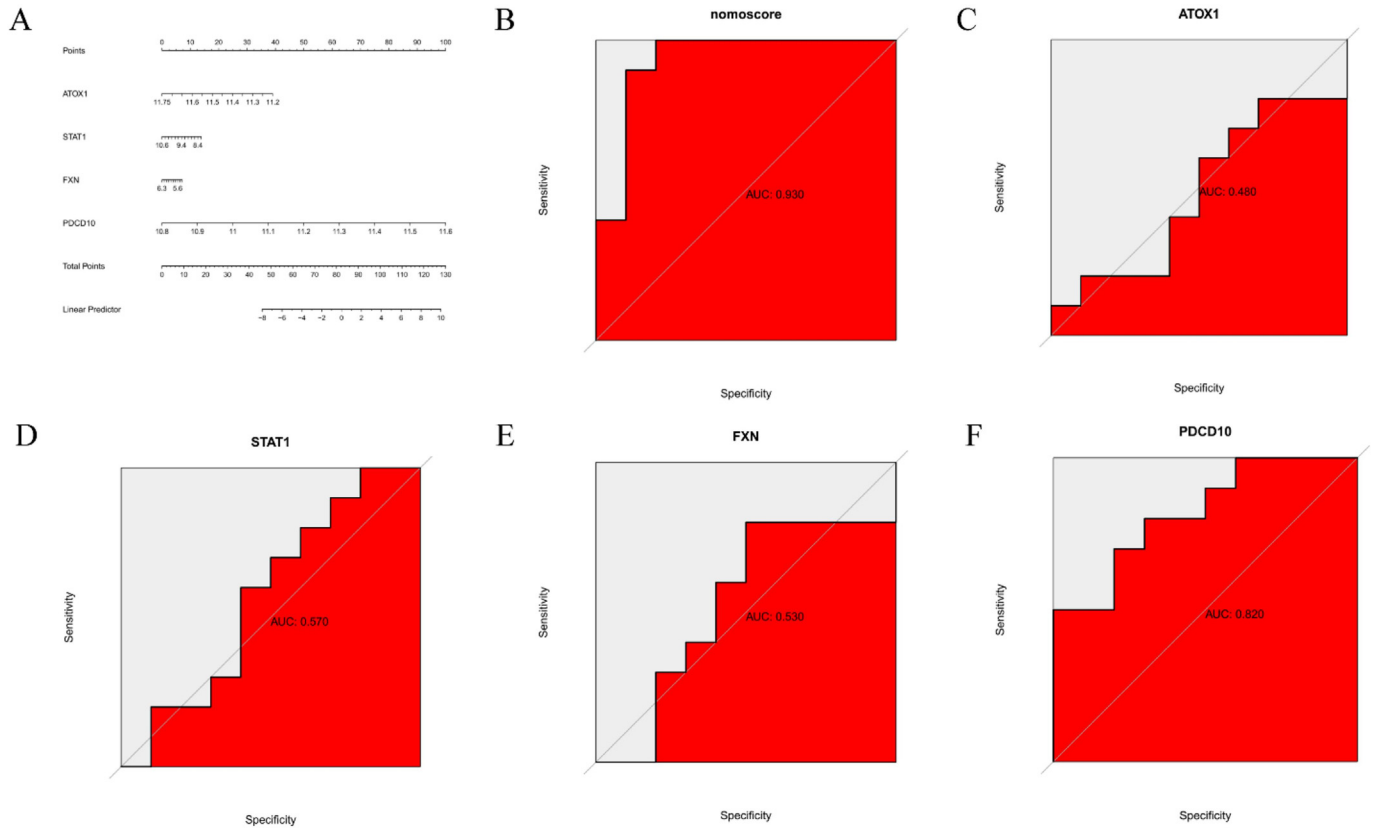

Fig. 7. External validation of the vitiligo risk prediction model using an independent public dataset. (A) Reconstructed diagnostic nomogram based on FG expression in the validation dataset. (B) ROC curve validation of the new diagnostic nomogram. (C–F) Individual ROC curves for *ATOX1*, *STAT1*, *FXN*, and *PDCD10* in the validation dataset. AUC interpretation: $0.5 \leq$ AUC < 0.7: low accuracy; $0.7 \leq$ AUC < 0.9: moderate accuracy; AUC ≥ 0.9: high accuracy.

known oxidative stress-related genes, resulting in 42 intersecting genes. These genes were significantly enriched in functions such as the mitochondrial matrix, antioxidant activity, response to oxidative stress, adipocytokine signaling, and prolactin signaling pathways. Machine learning algorithms, including LASSO, SVM-RFE, and RF, were employed to identify FGs from this intersection, which were then subjected to real-time PCR analysis for validation. Our results confirmed that *ATOX1*, *STAT1*, *FXN*, and *PDCD10* are FGs related to oxidative stress in vitiligo. We then constructed a risk prediction model based on the FGs, which demonstrated high accuracy, as validated by the ROC curve. Furthermore, we performed accuracy validation using the GSE65127 dataset, in which *PDCD10* emerged as the most accurate FG. Finally, Mendelian randomization analysis revealed that *ATOX1*, *STAT1*, and *PDCD10* had OR point estimates greater than 1, suggesting a potential association with increased vitiligo risk, whereas *FXN* showed the opposite trend, although none of these associations reached statistical significance.

Oxidative stress is widely acknowledged as an initial trigger in the development of vitiligo. In vitiligo patients, there is a substantial increase in ROS levels within the affected skin, with more pronounced elevations observed in advanced cases. These findings suggest that ROS neutralization can be a viable treatment approach [7,33]. During periods of stress, the buildup of ROS can perturb the cellular redox balance. This disruption can lead to the production of proinflammatory cytokines and the activation of signaling pathways detrimental to melanocytes. This phenomenon is referred to as damage-associated molecular patterns, which can be identified and bound by pattern recognition receptors (PRRs) [34,35]. Furthermore, when microorganisms invade the body, PRRs identify pathogen-associated molecular patterns (PAMPs). Double-stranded DNA originating from specific viruses or bacteria, along with lipopolysaccharides derived from bacterial cell walls, can act as ligands for PAMPs. Both of these mechanisms can trigger the innate immune system, leading to the apoptosis of melanocytes and keratinocytes. Common PRRs include Toll-like receptors (TLRs), RIG-I-like receptors (RLRs), and NOD-like receptors (NLRs) [36]. Notably, TLRs play a pivotal role in recognizing PAMPs and facilitating melanocyte apoptosis, a process closely intertwined with the pathogenesis of vitiligo [37]. For example, extracellular viral dsRNA can activate human melanocytes to produce TLR3, subsequently leading to autonomous IFN-β secretion and apoptosis [38]. Furthermore, lipopolysaccharides within bacterial cell walls can serve as ligands, triggering TLR4 activation and inducing autophagy in melanocytes, thus promoting vitiligo development [39,40]. Moreover, the RLR and NLR pathways contribute to innate immune activation, fostering vitiligo development. For example, IL-22 can induce the generation of ROS, subsequently activating the NLR family pyrin domain-containing protein 3 (NLRP3) pathway, thereby promoting the secretion of IL-1 by keratinocytes, which act as innate immune cells. This cascade reaction ultimately leads to the apoptosis of melanocytes [41]. In the context of vitiligo, congenital immunity plays a vital role in bridging the link between melanocyte stress and long-term adaptive immunity [42]. Furthermore, our GSEA enrichment analysis revealed a significant association between genes in the vitiligo lesion group and signaling pathways such as the NOD-like receptor, Toll-like receptor, and RIG-I-like receptor pathways. This finding aligns with earlier conclusions regarding the mechanism by which oxidative stress triggers an immune response leading to melanocyte damage. In addition, adaptive immunity plays a crucial role in melanocyte destruction. Dendritic cells have the capacity to present

melanocyte-associated antigen proteins, which are involved in melanin synthesis, to specific cytotoxic T cells, thereby eliciting the production of autoantibodies, TNF-α, and IFN-γ, ultimately culminating in melanocyte apoptosis [35,43,44]. Furthermore, the IFN-γ-mediated CXCL10-CXCR3 axis has been demonstrated to recruit CD8+ T cells, intensifying melanocyte depletion and ultimately contributing to the development of vitiligo-associated melanopenia [45,46,47]. Multiple studies have consistently indicated that oxidative stress can be regarded as the initiating factor in the melanocyte destruction mechanism, representing an early response observed in vitiligo patients [6,47,48].

DEG enrichment analysis revealed a close association between vitiligo and the mitochondrial matrix, ribosomes, and oxidative phosphorylation. Research has demonstrated that a reduction in mitochondrial ATP production significantly impairs melanocyte migration [49]. Analysis of enriched genes revealed the involvement of oxidative stress, mitochondria, chemical carcinogenesis, adipocytokine signaling, and prolactin signaling pathways in vitiligo. Chemical exposure frequently triggers the development of vitiligo, with monobenzone being the most well-known and FDA-approved depigmentation agent [50]. Lipid metabolism disorders are common in patients with vitiligo, and one of the genes preliminarily screened in this study, *APOD*, is implicated in a specific aspect of lipid metabolism. These findings suggest a potential link between adipocytokine signaling, oxidative stress, and vitiligo [51,52]. Research has demonstrated that the modulation of lipid metabolism can influence the secretion of immune cells and cytokines in vitiligo, thus alleviating the disease [53]. Moreover, the mechanism by which the herbal formula Kang-Bai-Ling treats vitiligo may involve targeting the prolactin signaling pathway, underscoring the need for further research on this pathway in vitiligo [54].

ATOX1 is an antioxidant encoding the copper transport protein antioxidant 1 and promotes cell survival by effectively reducing ROS production and minimizing DNA damage. It has demonstrated efficacy in treating diseases induced by oxidative stress and in enhancing neuronal protection against oxidative stress damage [55,56]. Additionally, preliminary findings in animal models suggest that *ATOX1* may alleviate damage induced by oxidative stress-associated ischemia [57]. *STAT1* is commonly linked with cellular damage. Oxidative stress induces the phosphorylation and S-glutathionylation of *STAT1*, leading to its abnormal activation and upregulation [58,59]. *FXN* depletion is closely linked to the oxygen environment [60]. Suppression of *FXN* expression can result in heightened iron buildup and mitochondrial oxidative stress responses. Recent research has shown that a deficiency in *FXN* increases ROS production due to the loss of aconitase activity, concurrently hindering DNA repair pathways. These factors synergistically contribute to mitochondrial dysfunction, culminating in cell death [61]. *PDCD10* is a protein associated with cell apoptosis that can increase cell antioxidant capacity and promote cell apoptosis under oxidative stress. *PDCD10* was upregulated in a ROS-dependent manner in tumor cells, including prostate cancer and pancreatic cancer cells. *PDCD10* enhances STK25-induced cell apoptosis under oxidative stress. However, the application of antioxidants can reduce ROS production and impede the functions of both *PDCD10* and STK25, consequently promoting cell survival [62]. *APOD* encodes apolipoprotein D, a lipid-binding protein within the lipoprotein family with lipid antioxidant function. Surprisingly, *APOD* is prominently expressed in neurons and has the ability to ameliorate early oxidative stress-induced damage [63]. Although *APOD* has been extensively investigated in neurological disorders, recent research has identified its role as an early oxidative stress response gene in colorectal cancer, where it is highly reactive. This finding suggests its potential utility as an early diagnostic marker for the tumor microenvironment [64]. Our research revealed the upregulation of *ATOX1*, *STAT1*, and *PDCD10* expression in vitiligo tissues, coupled with the downregulation of *FXN* and *APOD*. Therefore, we hypothesize that the increased expression of *ATOX1* and *APOD* may imply a protective response, potentially indicating a predictive role in the context of persistent oxidative stress. Nevertheless, experimental validation of *APOD* contradicted our initial bioinformatic prediction — real-time PCR showed significant upregulation rather than the expected downregulation. This discrepancy may be attributable to several factors, including differences between the tissue microenvironment of the clinical samples and the conditions represented in the public datasets, potential heterogeneity in patient populations (e.g., disease stage, treatment history), or platform-specific technical biases in gene expression measurement. Additionally, *APOD* expression is known to be highly context-dependent and influenced by local oxidative stress levels, lipid metabolism, and inflammatory signals, which may vary considerably between lesional skin in vivo and the samples captured in the GEO datasets [63,64]. Further investigations with larger sample sizes and stratified analyses are warranted to clarify the role of *APOD* in vitiligo. Moreover, the upregulation of *STAT1* and *PDCD10*, coupled with the downregulation of *FXN*, actively contributes to oxidative stress-induced melanocyte apoptosis in vitiligo, emphasizing their potential as targets for antioxidant-based therapeutic interventions. However, more extensive research is essential to corroborate the roles of these FGs in the oxidative stress mechanisms underlying vitiligo.

This study has several limitations. First, the diagnostic model achieved an AUC of 1.00 in the training dataset, which likely reflects overfitting, given the relatively small sample size (n = 20 per group). Although we validated the model using an independent external dataset (GSE65127), in which the AUC remained high at 0.93, formal internal validation strategies, such as repeated cross-validation or bootstrapping, were not applied during model construction. Future studies should incorporate such methods to rigorously assess model generalizability.

Second, while the combined four-gene model demonstrated strong predictive performance in external validation (AUC = 0.93), three of the four individual FGs (*ATOX1*, *STAT1*, and *FXN*) showed weak discriminatory performance (AUC values of 0.480, 0.570, and 0.530, respectively) in the GSE65127 dataset. Only *PDCD10* maintained an acceptable individual accuracy (AUC = 0.820). This suggests that the predictive power of the model is driven by the synergistic contribution of all four genes, and no single gene alone, with the possible exception of *PDCD10*, is sufficient as a standalone biomarker. This pattern also underscores the importance of multi-gene panel approaches in complex multifactorial diseases, such as vitiligo.

Third, the risk prediction nomogram was constructed solely based on gene expression data without incorporating clinical covariates such as age at onset, disease duration, or lesion extent. This design choice was deliberate, as the primary aim of this study was to evaluate the independent predictive value of oxidative stress-related gene expression signatures. However, future translational models should integrate molecular and clinical variables to enhance their clinical applicability.

Fourth, the Mendelian randomization analysis yielded OR point estimates consistent with the hypothesized directions of effect, but none reached statistical significance as all 95% CIs crossed 1. This may be attributed to the limited power resulting from the small number of strong instrumental variables available for each gene. Future MR studies with larger GWAS datasets and stronger instruments are needed to confirm or refute these associations.

Finally, the sample size for the real-time PCR validation was limited (n = 12 pairs). Larger validation cohorts with detailed clinical phenotyping are required to confirm these findings.

5. Conclusions

In conclusion, the onset and progression of vitiligo are intricately associated with oxidative stress and immune response. This study employed a multifaceted approach involving bioinformatics, machine learning, and Mendelian randomization to identify *ATOX1*, *STAT1*, *FXN*, and *PDCD10* as FGs associated with oxidative stress in vitiligo. Moreover, we facilitated future vitiligo diagnosis and provided a scientific foundation for risk assessment and treatment. Nonetheless, future research should entail additional experimental investigations with larger sample sizes and multi-center cohorts to elucidate the precise roles of these FGs in the initiation and progression of vitiligo.

CRediT authorship contribution statement

Yuan Xia: Writing – original draft, Visualization, Validation, Software, Resources, Methodology, Investigation, Formal analysis, Data curation, Conceptualization. **Lin Liu:** Methodology. **Hucheng Zhou:** Formal analysis. **Lingli Fang:** Resources. **Yanyan Chen:** Software. **Hengheng Fan:** Investigation. **Yuyun Xiong:** Formal analysis. **Yumei Li:** Writing – review & editing, Visualization, Validation, Supervision, Software, Resources, Project administration, Methodology, Investigation, Funding acquisition, Formal analysis, Data curation, Conceptualization.

Informed consent

Informed consent was obtained from each of the patients involved in the study.

Ethical approval

This study was approved by the Ethics Committee of the Affiliated Hospital of Jiangsu University, and the Declaration of Helsinki guidelines were followed (project identification code KY2023K1106).

Financial support

This work was supported by the Postgraduate Research & Practice Innovation Program of Jiangsu Province (SJCX24_2450) and Jiangsu Provincial Medical Key Discipline Cultivation Unit (JSDW202229).

Data availability

The publicly available datasets analyzed in this study were accessed from the Gene Expression Omnibus (GEO) repository (https://www.ncbi.nlm.nih.gov/geo/) under accession numbers GSE75819, GSE53146, and GSE65127. Mendelian randomization data were obtained from the IEU OpenGWAS project (https://gwas.mrcieu.ac.uk/) using the following GWAS IDs: eqtl-a-ENSG00000177556 (*ATOX1*), eqtl-a-ENSG00000115415 (*STAT1*), eqtl-a-ENSG00000165060 (*FXN*), and eqtl-a-ENSG00000114209 (*PDCD10*). Additional datasets generated and analyzed during the current study are available from the corresponding author upon reasonable request.

Declaration of competing interests

The authors declare that they have no known competing financial interests or personal relationships that could have appeared to influence the work reported in this paper.

Appendix A. Supplementary material

Supplementary data to this article can be found online at https://doi.org/10.1016/j.ejbt.2026.100724.

References

[1] AL-smadi K, Imran M, Leite-Silva VR, et al. Vitiligo: A review of aetiology, pathogenesis, treatment, and psychosocial impact. Cosmetics 2023;10(3):84. https://doi.org/10.3390/cosmetics10030084.
[2] Xu W, Qiu Z, Li C, et al. Recurrence and risk factors in cured patients with vitiligo: A real-life single-center retrospective study. J Cosmet Dermatol 2023;22(5):1680–4. https://doi.org/10.1111/jocd.15637. PMid: 36721299.
[3] Spritz RA, Santorico SA. The genetic basis of vitiligo. J Invest Dermatol 2021;141(2):265–73. https://doi.org/10.1016/j.jid.2020.06.004. PMid: 32778407.
[4] Roberts GHL, Santorico SA, Spritz RA. Deep genotype imputation captures virtually all heritability of autoimmune vitiligo. Hum Mol Genet 2020;29(5):859–63. https://doi.org/10.1093/hmg/ddaa005. PMid: 31943001.
[5] Bergqvist C, Ezzedine K. Vitiligo: A focus on pathogenesis and its therapeutic implications. J Dermatol 2021;48(3):252–70. https://doi.org/10.1111/1346-8138.15743. PMid: 33404102.
[6] Li S, Zhu G, Yang Y, et al. Oxidative stress drives $CD8^+$ T-cell skin trafficking in patients with vitiligo through CXCL16 upregulation by activating the unfolded protein response in keratinocytes. J Allergy Clin Immunol 2017;140(1):177–189.e9. https://doi.org/10.1016/j.jaci.2016.10.013. PMid: 27826097.
[7] Zhang J, Hu W, Wang P, et al. Research progress on targeted antioxidant therapy and vitiligo. Oxidative Med Cell Longevity 2022;2022:1821780. https://doi.org/10.1155/2022/1821780. PMid: 35320978.
[8] Chen J, Li S, Li C. Mechanisms of melanocyte death in vitiligo. Med Res Rev 2021;41(2):1138–66. https://doi.org/10.1002/med.21754. PMid: 33200838.
[9] Xu X, Zhang C, Jiang M, et al. Impact of treatment delays on vitiligo during the COVID-19 pandemic: A retrospective study. Dermatol Ther 2021;34(4):e15014. https://doi.org/10.1111/dth.15014. PMid: 34075666.
[10] Mohammadi S, Amiri R, Khalili M, et al. Treatment protocols and efficacy of combined laser with medical treatment modalities in vitiligo. J Cosmet Dermatol 2022;21(8):3272–91. https://doi.org/10.1111/jocd.14602. PMid: 34766697.
[11] Zhang J, Yu R, Guo X, et al. Identification of TYR, TYRP1, DCT and LARP7 as related biomarkers and immune infiltration characteristics of vitiligo via comprehensive strategies. Bioengineered 2021;12(1):2214–27. https://doi.org/10.1080/21655979.2021.1933743. PMid: 34107850.
[12] Miao Y, Su D, Fu Q, et al. Identification of CKS2 and RRM2 as potential markers of vitiligo using bioinformatics analysis. Medicine 2022;101(46):e31908. https://doi.org/10.1097/MD.0000000000031908. PMid: 36401415.
[13] Li S, Dai W, Wang S, et al. Clinical significance of serum oxidative stress markers to assess disease activity and severity in patients with non-segmental vitiligo. Front Cell Dev Biol 2021;9:739413. https://doi.org/10.3389/fcell.2021.739413. PMid: 34977005.
[14] Atas H, Kocabiyik M, Gonul M, et al. Usefulness of ischemia-modified albumin in predicting oxidative stress in patients with vitiligo. Biomark Med 2017;11(6):439–49. https://doi.org/10.2217/bmm-2016-0259. PMid: 28598198.
[15] Frisoli ML, Essien K, Harris JE. Vitiligo: Mechanisms of pathogenesis and treatment. Annu Rev Immunol 2020;38(1):621–48. https://doi.org/10.1146/annurev-immunol-100919-023531. PMid: 32017656.
[16] Guarneri F, Bertino L, Pioggia G, et al. Therapies with antioxidant potential in psoriasis, vitiligo, and lichen planus. Antioxidants 2021;10(7):1087. https://doi.org/10.3390/antiox10071087. PMid: 34356320.
[17] Karagaiah P, Valle Y, Sigova J, et al. Emerging drugs for the treatment of vitiligo. Expert Opin Emerg Drugs 2020;25(1):7–24. https://doi.org/10.1080/14728214.2020.1712358. PMid: 31958256.
[18] Lee JH, Kwon HS, Jung HM, et al. Treatment outcomes of topical calcineurin inhibitor therapy for patients with vitiligo: A systematic review and meta-analysis. JAMA Dermatol 2019;155(8):929–38. https://doi.org/10.1001/jamadermatol.2019.0696. PMid: 31141108.
[19] Chang HC, Hsu YP, Huang YC. The effectiveness of topical calcineurin inhibitors compared with topical corticosteroids in the treatment of vitiligo: A systematic review and meta-analysis. J Am Acad Dermatol 2020;82(1):243–5. https://doi.org/10.1016/j.jaad.2019.07.108. PMid: 31408687.
[20] Zhou Y, Khan M, Jiang L, et al. The current status of antioxidants in the treatment of vitiligo in China. Oxidative Med Cell Longevity 2022;2022:2994558. https://doi.org/10.1155/2022/2994558. PMid: 35251468.
[21] Barrett T, Wilhite SE, Ledoux P, et al. NCBI GEO: Archive for functional genomics data sets—update. Nucleic Acids Res 2013;41(D1):D991–5. https://doi.org/10.1093/nar/gks1193. PMid: 23193258.
[22] Leek JT, Johnson WE, Parker HS, et al. The sva package for removing batch effects and other unwanted variation in high-throughput experiments. Bioinformatics 2012;28(6):882–3. https://doi.org/10.1093/bioinformatics/bts034. PMid: 22257669.
[23] Ritchie ME, Phipson B, Wu D, et al. *limma powers* differential expression analyses for RNA-sequencing and microarray studies. Nucleic Acids Res 2015;43(7):e47. https://doi.org/10.1093/nar/gkv007. PMid: 25605792.

[24] Subramanian A, Tamayo P, Mootha VK, et al. Gene set enrichment analysis: A knowledge-based approach for interpreting genome-wide expression profiles. PNAS 2005;102(43):15545–50. https://doi.org/10.1073/pnas.0506580102. PMid: 16199517.
[25] Ashburner M, Ball CA, Blake JA, et al. Gene ontology: Tool for the unification of biology. Nat Genet 2000;25(1):25–9. https://doi.org/10.1038/75556. PMid: 10802651.
[26] Kanehisa M, Goto S. KEGG: Kyoto encyclopedia of genes and genomes. Nucleic Acids Res 2000;28(1):27–30. https://doi.org/10.1093/nar/28.1.27. PMid: 10592173.
[27] Yu G, Wang LG, Han Y, et al. clusterProfiler: An R Package for comparing biological themes among gene clusters. OMICS: J Integrative Biol 2012;16 (5):284–7. https://doi.org/10.1089/omi.2011.0118. PMid: 22455463.
[28] Carbon S, Ireland A, Mungall CJ, et al. AmiGO: Online access to ontology and annotation data. Bioinformatics 2009;25(2):288–9. https://doi.org/10.1093/bioinformatics/btn615. PMid: 19033274.
[29] Saeys Y, Inza I, Larrañaga P. A review of feature selection techniques in bioinformatics. Bioinformatics 2007;23(19):2507–17. https://doi.org/10.1093/bioinformatics/btm344. PMid: 17720704.
[30] Parsad D, Gupta S. Standard guidelines of care for vitiligo surgery. Indian J Dermatol Venereol Leprol 2008;74(7):37–45. PMid: 18688102.
[31] Lin Z, Qi R, Deng H, et al. Bidirectional mendelian randomization suggests causal effects of 731 immunophenotypes on vitiligo pathogenesis. Clin Cosmet Investig Dermatol 2026;19:603361. https://doi.org/10.2147/CCID.S603361. PMid: 42145868.
[32] Hemani G, Zheng J, Elsworth B, et al. The MR-Base platform supports systematic causal inference across the human phenome. Elife 2018;7: e34408. https://doi.org/10.7554/eLife.34408. PMid: 29846171.
[33] Dell'Anna ML, Maresca V, Briganti S, et al. Mitochondrial impairment in peripheral blood mononuclear cells during the active phase of vitiligo. J Invest Dermatol 2001;117(4):908–13. https://doi.org/10.1046/j.0022-202x.2001.01459.x. PMid: 11676831.
[34] Boniface K, Passeron T, Seneschal J, et al. Targeting innate immunity to combat cutaneous stress: The vitiligo perspective. Front Immunol 2021;12:613056. https://doi.org/10.3389/fimmu.2021.613056. PMid: 33936032.
[35] Khaitan BK, Sindhuja T. Autoimmunity in vitiligo: Therapeutic implications and opportunities. Autoimmun Rev 2022;21(1):102932. https://doi.org/10.1016/j.autrev.2021.102932. PMid: 34506987.
[36] Wang Y, Li S, Li C. Perspectives of new advances in the pathogenesis of vitiligo: From oxidative stress to autoimmunity. Med Sci Monitor 2019;25:1017–23. https://doi.org/10.12659/MSM.914898. PMid: 30723188.
[37] Abdelsalam M, Allam SH, Zohdy M, et al. TLR4 gene polymorphisms in Egyptian vitiligo patients: Insights into emerging association with clinical activity, family history, and response to therapy. J Genet Eng Biotechnol 2021;19(1):132. https://doi.org/10.1186/s43141-021-00218-y. PMid: 34468896.
[38] Yu N, Zhang S, Sun T, et al. Double-stranded RNA induces melanocyte death via activation of Toll-like receptor 3. Exp Dermatol 2011;20(2):134139. https://doi.org/10.1111/j.1600-0625.2010.01208.x. PMid: 21255093.
[39] Sun L, Sun J, Huo X, et al. Lipopolysaccharide reduces melanin synthesis in vitiligo melanocytes by regulating autophagy. Exp Dermatol 2022;31 (10):1579–85. https://doi.org/10.1111/exd.14629. PMid: 35733278.
[40] Song PI, Abraham TA, Park Y, et al. The expression of functional LPS receptor proteins CD14 and toll-like receptor 4 in human corneal cells. Invest Ophthalmol Vis Sci 2001;42(12):2867–77. PMid: 11687531.
[41] Dong J, An X, Zhong H, et al. Interleukin-22 participates in the inflammatory process of vitiligo. Oncotarget 2017;8(65):109161–74. https://doi.org/10.18632/oncotarget.22644. PMid: 29312598.
[42] Shi F, Kong BW, Song JJ, et al. Understanding mechanisms of vitiligo development in Smyth line of chickens by transcriptomic microarray analysis of evolving autoimmune lesions. BMC Immunol 2012;13:18. https://doi.org/10.1186/1471-2172-13-18. PMid: 22500953.
[43] Ungureanu L, Vasilovici AF, Halmagyi SR, et al. The many faces of autoimmune-mediated melanocyte destruction in melanoma. Front Immunol 2024;15:1417273. https://doi.org/10.3389/fimmu.2024.1417273. PMid: 39421737.
[44] Strassner JP, Harris JE. Understanding mechanisms of autoimmunity through translational research in vitiligo. Curr Opin Immunol 2016;43:81–8. https://doi.org/10.1016/j.coi.2016.09.008. PMid: 27764715.
[45] Yang L, Wei Y, Sun Y, et al. Interferon-gamma inhibits melanogenesis and induces apoptosis in melanocytes: A pivotal role of $CD8^+$ cytotoxic T lymphocytes in vitiligo. Acta Derm Venereol 2015;95(6):664–70. https://doi.org/10.2340/00015555-2080. PMid: 25721262.
[46] Rashighi M, Agarwal P, Richmond JM, et al. CXCL10 is critical for the progression and maintenance of depigmentation in a mouse model of vitiligo. Sci Transl Med 2014;6(223):223ra23. https://doi.org/10.1126/scitranslmed.3007811. PMid: 24523323.
[47] Wang XX, Wang QQ, Wu JQ, et al. Increased expression of CXCR3 and its ligands in patients with vitiligo and CXCL10 as a potential clinical marker for vitiligo. Br J Dermatol 2016;174(6):1318–26. https://doi.org/10.1111/bjd.14416. PMid: 26801009.
[48] He S, Xu J, Wu J. The promising role of chemokines in vitiligo: From oxidative stress to the autoimmune response. Oxid Med Cell Longev 2022;2022:8796735. https://doi.org/10.1155/2022/8796735. PMid: 35096274.
[49] Xu P, Xue YN, Ji HH, et al. H_2O_2-induced oxidative stress disrupts mitochondrial functions and impairs migratory potential of human epidermal melanocytes. Exp Dermatol 2020;29(8):733–41. https://doi.org/10.1111/exd.14134. PMid: 32580253.
[50] Wang Y, Li S, Li C. Clinical features, immunopathogenesis, and therapeutic strategies in vitiligo. Clin Rev Allergy Immunol 2021;61(3):299–323. https://doi.org/10.1007/s12016-021-08868-z. PMid: 34283349.
[51] Page S, Chandhoke V, Baranova A. Melanin and melanogenesis in adipose tissue: Possible mechanisms for abating oxidative stress and inflammation? Obes Rev 2011;12(5):e21–31. https://doi.org/10.1111/j.1467-789X.2010.00773.x. PMid: 20576005.
[52] Tanacan E, Atakan N. Higher incidence of metabolic syndrome components in vitiligo patients: A prospective cross-sectional study. An Bras Dermatol 2020;95(2):165–72. https://doi.org/10.1016/j.abd.2019.07.006. PMid: 32113676.
[53] Wu M, Wang L, Wu H, et al. *Leptin* deficiency in $CD8^+$ T cells ameliorates non-segmental vitiligo by reducing interferon-gamma and Granzyme B. Front Immunol 2023;14:1158883. https://doi.org/10.3389/fimmu.2023.1158883. PMid: 37207234.
[54] Xu M, Shi J, Min Z, et al. A network pharmacology approach to uncover the molecular mechanisms of herbal formula Kang-bai-ling for treatment of vitiligo. Evid Based Complement Alternat Med 2019;2019:3053458. https://doi.org/10.1155/2019/3053458. PMid: 31781265.
[55] Vo TTT, Peng TY, Nguyen TH, et al. The crosstalk between copper-induced oxidative stress and cuproptosis: A novel potential anticancer paradigm. Cell Commun Signaling 2024;22(1):353. https://doi.org/10.1186/s12964-024-01726-3. PMid: 38970072.
[56] Yang D, Xiao P, Qiu B, et al. Copper chaperone antioxidant 1: Multiple roles and a potential therapeutic target. J Mol Med 2023;101(5):527–42. https://doi.org/10.1007/s00109-023-02311-w. PMid: 37017692.
[57] Sudhahar V, Shi Y, Kaplan JH, et al. Whole-transcriptome sequencing analyses of nuclear antioxidant-1 in endothelial cells: Role in inflammation and atherosclerosis. Cells 2022;11(18):2919. https://doi.org/10.3390/cells11182919. PMid: 36139494.
[58] Jin W, Zhao J, Yang E, et al. Neuronal STAT3/HIF-1α/PTRF axis-mediated bioenergetic disturbance exacerbates cerebral ischemia-reperfusion injury via PLA2G4A. Theranostics 2022;12(7):3196–216. https://doi.org/10.7150/thno.71029. PMid: 35547748.
[59] Butturini E, Carcereri de Prati A, Mariotto S. Redox regulation of STAT1 and STAT3 signaling. Int J Mol Sci 2020;21(19):7034. https://doi.org/10.3390/ijms21197034. PMid: 32987855.
[60] Ast T, Meisel JD, Patra S, et al. Hypoxia rescues frataxin loss by restoring iron sulfur cluster biogenesis. Cell 2019;177(6):1507–1521e16. https://doi.org/10.1016/j.cell.2019.03.045. PMid: 31031004.
[61] Moreno-Lorite J, Pérez-Luz S, Katsu-Jiménez Y, et al. DNA repair pathways are altered in neural cell models of frataxin deficiency. Mol Cell Neurosci 2021;111:103587. https://doi.org/10.1016/j.mcn.2020.103587. PMid: 33418083.
[62] Valentino M, Dejana E E, Malinverno M. The multifaceted *PDCD10/CCM3* gene. Genes Dis 2021;8(6):798–813. https://doi.org/10.1016/j.gendis.2020.12.008. PMid: 34522709.
[63] Bajo-Grañeras R, Sanchez D, Gutierrez G, et al. Apolipoprotein D alters the early transcriptional response to oxidative stress in the adult cerebellum. J Neurochem 2011;117(6):949–60. https://doi.org/10.1111/j.1471-4159.2011.07266.x. PMid: 21463325.
[64] Bajo-Grañeras R, Crespo-Sanjuan J, García-Centeno RM, et al. Expression and potential role of apolipoprotein D on the death-survival balance of human colorectal cancer cells under oxidative stress conditions. Int J Colorectal Dis 2013;28(6):751–66. https://doi.org/10.1007/s00384-012-1616-2. PMid: 23296401.